Velocity and pressure fluctuations induced by the precessing helical vortex in a conical diffuser

A Javadi[1], A Bosioc[2], H Nilsson[1], S Muntean[3], R Susan-Resiga[2,3]
[1] Department of Applied Mechanics, Chalmers University of Technology, SE-412 96 Gothenburg, Sweden
[2] Department of Hydraulic Machinery, University Politehnica Timisoara, Bv. Mihai Viteazu, No. 1, Ro-300222, Timisoara, Romania
[3]Center for Advanced Research in Engineering Sciences, Romanian Academy – Timisoara Branch, Bv. MihaiViteazu, No. 24, Ro-300223, Timisoara, Romania

E-mail: ardalan.javadi@chalmers.se

Abstract. The flow unsteadiness generated in the draft tube cone of hydraulic turbines affects the turbine operation. Therefore, several swirling flow configurations are investigated using a swirling apparatus in order to explore the unsteady phenomena. The swirl apparatus has two parts: the swirl generator and the test section. The swirl generator includes two blade rows being designed such that the exit velocity profile resembles that of a turbine with fixed pitch. The test section includes a divergent part similar to the draft tube cone of a Francis turbine. A new control method based on a magneto rheological brake is used in order to produce several swirling flow configurations. As a result, the investigations are performed for six operating regimes in order to quantify the flow from part load operation, corresponding to runaway speed, to overload operation, corresponding to minimum speed, at constant guide vane opening. The part load operation corresponds to 0.7 times the best efficiency discharge, while the overload operation corresponds to 1.54 times the best efficiency discharge. LDV measurements are performed along three survey axes in the test section. The first survey axis is located just downstream the runner in order to check the velocity field at the swirl generator exit, while the next two survey axes are located at the inlet and at the outlet of the draft tube cone. Two velocity components are simultaneously measured on each survey axis. The measured unsteady velocity components are used to validate the results of unsteady numerical simulations, conducted using the OpenFOAM CFD code. The computational domain covers the entire swirling apparatus, including strouts, guide vanes, runner, and the conical diffuser. A dynamic mesh is used together with sliding GGI interfaces to include the effect of the rotating runner. The Reynolds averaged Navier–Stokes equations coupled with the RNG k–ε turbulence model are utilized to simulate the unsteady turbulent flow throughout the swirl generator.

1. Introduction

Confined swirling flow is found in numerous technical applications. The effects of the swirl may be favourable[1] or an unavoidable, possibly unforeseen, side effects which comprise a forced vortex core centred on its axis of rotation [2]. Vortex breakdown arises when a flow with some initial angular momentum is allowed to decay along the length of a tube. The vortex breakdown may cause severe pressure fluctuations that may damage the construction. In hydraulic turbines, such pressure pulsation appear in the draft tube at off-design operation and is associated with low-frequency phenomena developing in swirling flows [3]. For example, working at partial discharge the self-induced instability of the decaying swirling flow downstream the runner blade forms a precessing helical vortex, also called *vortex rope*. It is accompanied by strong pressure fluctuations [4-5] leading to severe physical damage[6].The mean swirl profiles develop through the diffusing draft tube, and may approach unstable conditions that cause a vortex breakdown [7-8].

It is known that a moderate level of residual swirl downstream the runner delays boundary layer separation at the draft tube wall and thus aids the pressure recovery. Large swirl intensities, however,

can degrade the performance by forming recirculation regions within the core flow [2]. Clausen *et al.* [9] found that there is a small range of swirl numbers that avoids both recirculation and separation.The characteristics of various breakdown states, or modes, in swirling flows depend on the swirl number

$$Sr = \frac{1}{R}\frac{\int_{R1}^{R2} r^2 UWdr}{\int_{R1}^{R2} rU^2 dr}, \qquad (1)$$

the Reynolds number (*Re*), and geometry-induced axial pressure gradients in the flow.

Here, R is the radius, W is the axial velocity and U is the tangential velocity. The inclusion of a slight inlet swirl (Sr=0.1) can reduce the precession speed, and may cause the helical precession to be against the mean swirl [10]. Several modes of precession are predicted as the swirl intensity increases, in which the helical precession, as well as the spiral structure, reverses the direction [11]. When the swirl increases to Sr=0.5, a central recirculation zone occurs, which is a typical manifestation of vortex breakdown [10]. This central reversed flow is the result of a low-pressure zone created by the centrifugal force.

A swirl generator apparatus was built at Politehnica University of Timisoara in order to investigate swirling flows and to develop novel flow control methods. The swirl generator delivers a swirling flow similar to that of a Francis runner operating at 70% partial discharge [12]. Downstream the runner a conical test section is installed, with the same angle as a real draft tube cone. The central recirculation zone from the conical diffuser was numerically investigated by Muntean *et al.*[13]. As a result, two flow control methods were experimentally investigated by Bosioc *et al.*[8] and Tănasă *et al.*[9] in order to mitigate the pressure fluctuations associated to the central zone.

To supplement experimental studies, it is desirable to increase the knowledge of swirling flow and vortex breakdown by using computational fluid dynamics (CFD). Unsteady Reynolds-averaged Navier-Stokes (URANS) simulations are practical and affordable tool to investigate and capture the main feature of the hydro turbine flow field [14]. Such turbulence models are justified in unsteady flow only if the scales associated with the resolved unsteady motion are substantially larger than the scales of the modelled turbulence. This condition may be satisfied in the large-scale and low-frequency dynamics of draft tube surge., When more details of the flow unsteadiness need to be captured, the LES and DES methodologies should be used [15].

In the present paper, unsteady three-dimensional turbulent flow throughout the Timisoara Swirl generator is investigated experimentally and numerically, to elucidate the effects of the swirl on the characteristics of the precessing helical vortex and vortex breakdown. A new control method based on magneto rheological brake is used in order to produce several swirling flow configurations. As a result, the investigations are performed for six operating regimes in order to quantify the flow from part load operation, corresponding to runaway speed, to overload operation, corresponding to minimum speed, at constant guide vane opening. The LDV measurements of the velocity are validated by numerical simulation using RNG k-ε turbulence modelling, and the flow is visualised by the numerical results.

2. Swirling flow apparatus and experimental details

The test rig consists of a main circuit used to supply the water to the swirling flow apparatus, Fig.1. The main centrifugal pump with variable speed provides up to 35 l/s. The swirl apparatus consists of a swirl generator and a convergent-divergent test section. The swirl generator consists of four leaned strouts, 13 guide vanes and a runner with 10 blades. The guide vanes create a tangential velocity component, while keeping practically a constant pressure. The purpose of the runner is to re-distribute the total pressure by inducing an excess in the axial velocity near the shroud and a corresponding deficit near the hub, like a Francis turbine operation at partial discharge. The runner blades act like a turbine near the hub, and a pump near the shroud. A special acquisition system was designed and implemented in order to measure the runner speed [16].

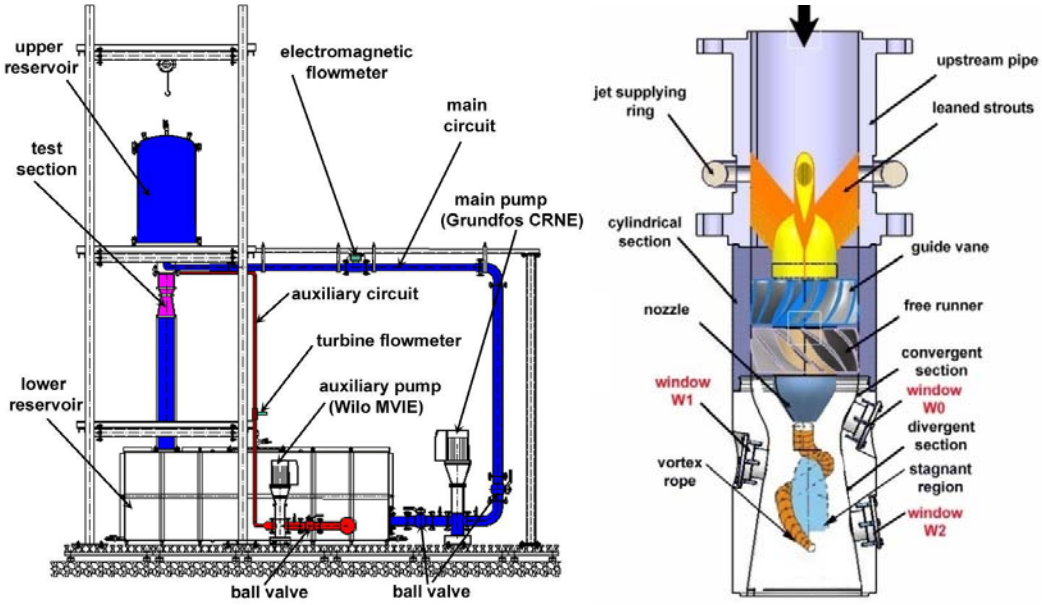

Figure 1. Closed loop test rig for experimental investigations of swirling flow installed at Politehnica University of Timisoara (left) and a cross section through the test section (right).

In order to decrease the speed, a magneto-rheological brake (MRB) was designed and installed on the runner [17]. The MRB device facilitates investigations of several experimental operating regimes, for validation of numerical results. Table 1 presents the operating conditions of the experimental test rig.

Table 1. Operating conditions of experimental test rig

Flow rate from the main circuit [l/sec]	30
Runner speed [*rpm*]	925, 800, 700, 600, 500, 400
Relative pressure in test rig [bar]	0.5

2.1. Velocity and pressure measurements

The experimental data are measured using a two-component Laser-Doppler Velocimetry (LDV) system using 10 μm aluminium tracer particles. The velocity measurements are realized in three different optical windows. The first window, W0, is located in the convergent part of the test section, and the other two windows, W1 and W2, are placed in the conical diffuser, see Fig. 2. Along survey axis W0, 31 points are measured while 113 and 141 points are considered at survey axes W1 and W2, respectively. The constant flow rate of 30 l/s during the measurements while the rotational speed of the runner is modified from 925rpm to 400 rpm. In each point on the survey axis, 50000 samples are measured during 20 seconds acquisition time. The dimensionless form of the velocity profiles is obtained using the bulk velocity in the throat section,

$$W_{\text{Throat}} = \frac{Q}{\pi R_{\text{Throat}}^2}.$$

The dimensionless length along each survey axis is obtained using the throat radius R_{Throat}=0.05 m.

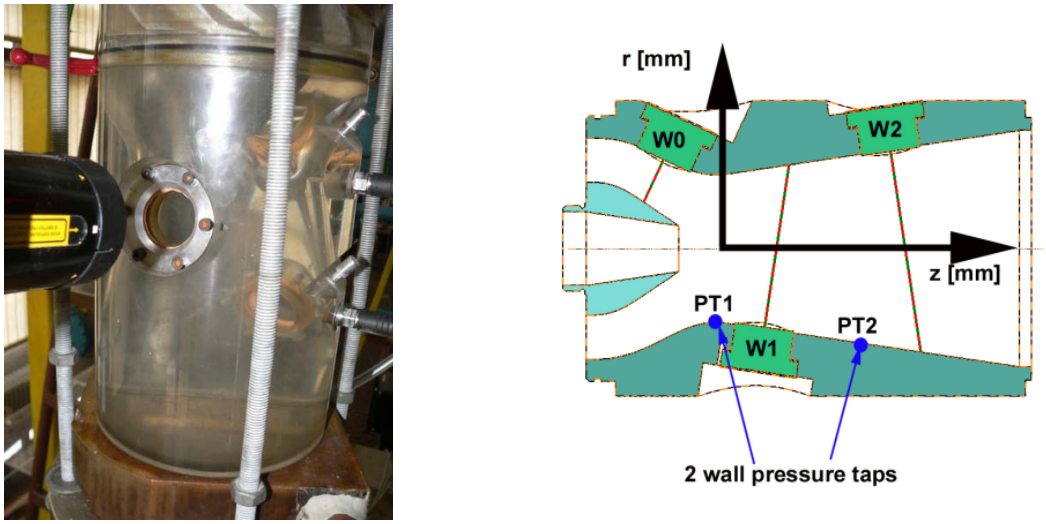

Figure 2. Test section mounted on the test rig with measuring windows and pressure taps (left)and sketch with positioning of survey axis W0, W1, W2 andPT1, PT2 pressure taps.

The unsteady static pressure is measured simultaneously with the LDV velocity profiles. The unsteady pressure is recorded on the cone wall on two points named PT1 and PT2, see Fig. 2. The first tap PT1 is located in the throat section while the pressure tap PT2 is placed 100 *mm* downstream in the conical diffuser with respect to the throat section. Two piezoresistive transducers from Kistler, model 4043A2, are used, with absolute pressure domain between 0 and 2 bars and natural frequency larger than 30 *kHz*. During the measurements, the acquisition frequency was approximately 1000 *Hz*. The reference signal from the throat was used as the trigger in the phase average procedure. One full vortex rope revolution is divided in 180 bins with 2 degrees on each bin.

3. Numerical setup

The structured hexahedral mesh is generated in the computation domain throughout the full scale flow passage of the swirl generator. The calculations reported herein are performed using the finite-volume method in the OpenFOAM open source CFD code. The second-order central difference scheme is used to discretize the diffusion terms, and the second-order linear-upwind difference scheme is adopted to approximate the convection term. The time-marching is performed with an implicit second-order accurate backward scheme. The computational domain is shown in Fig. 3,which includes the strout, the guide vanes, the runner, and the conical diffuser. The mesh comprises 2.08×10^{6} cells, with only 367 cells with angles less than 25 degrees. The General Grid Interface (GGI) [18] is used at the interfaces between the rotor and the stator. The main advantage of the GGI is that it allows non-conformal meshes at the interface. It makes mesh generation easier for complex geometries, and facilitates a sliding grid approach. It has been shown to give a close agreement for the velocity results between non-conformal and conformal meshes. The maximum CFL number is 1.25 for the runaway speed, which corresponds to 0.25 degrees runner rotation per time step. A constant velocity is specified at the strout inlet. A homogenous Neumann boundary condition is applied at the outlet for all variables.

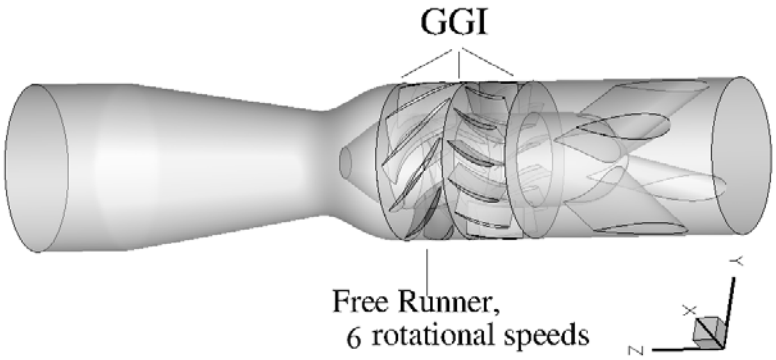

Figure3. Computational domain and GGI applied on interfaces.

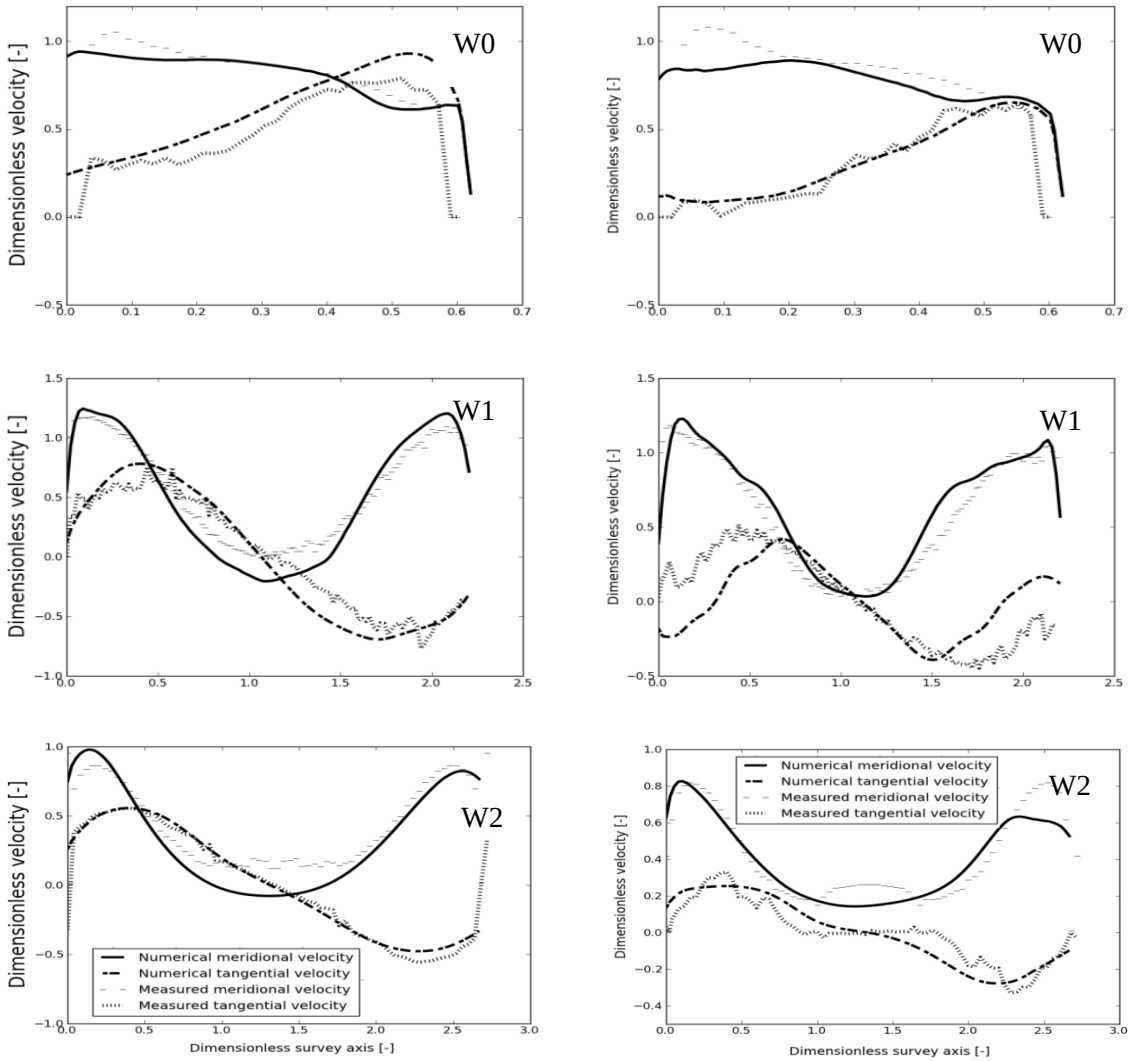

a) 400 *rpm* b) 500 *rpm*

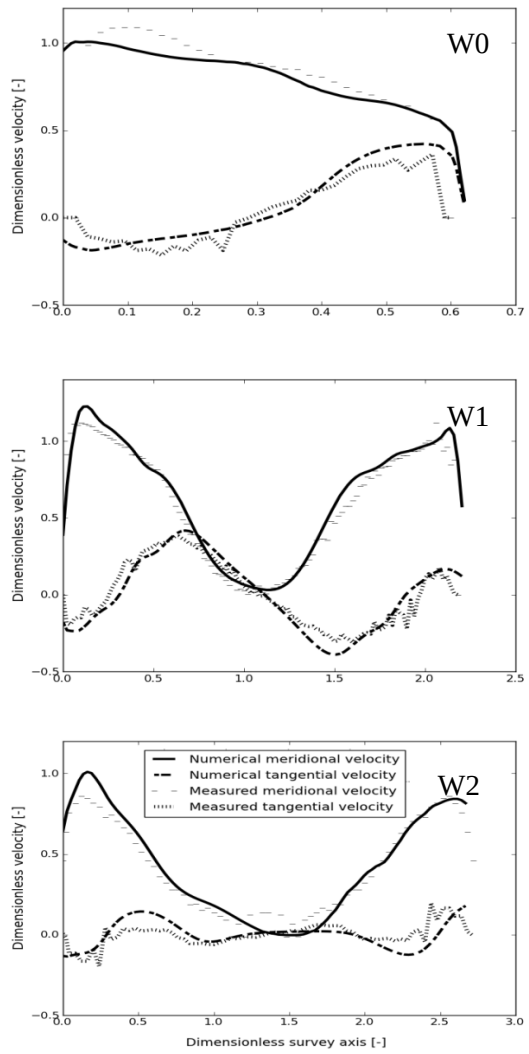

c) 600 *rpm*

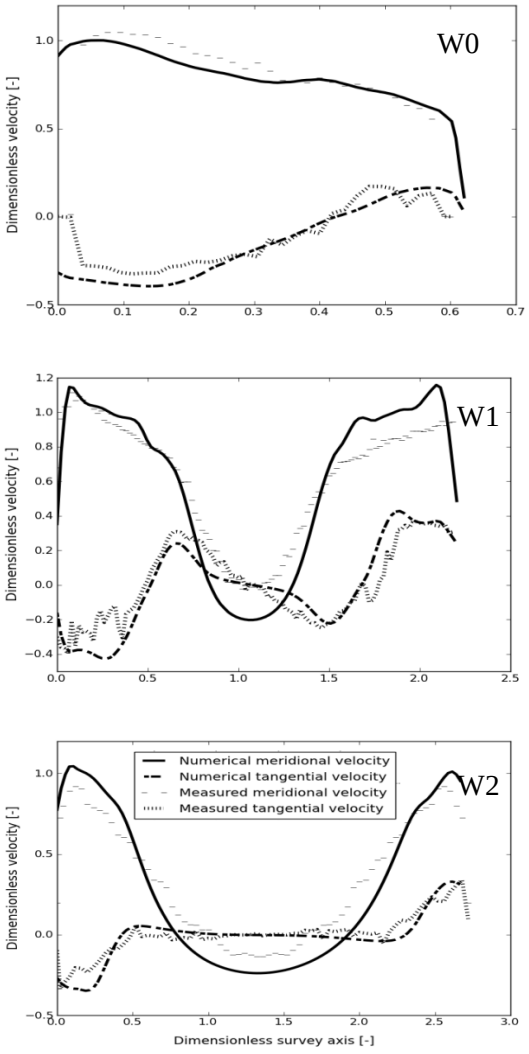

d) 700 *rpm*

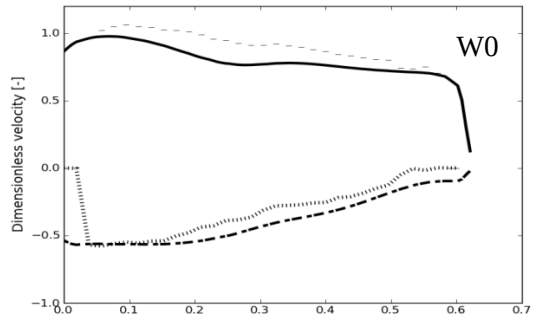

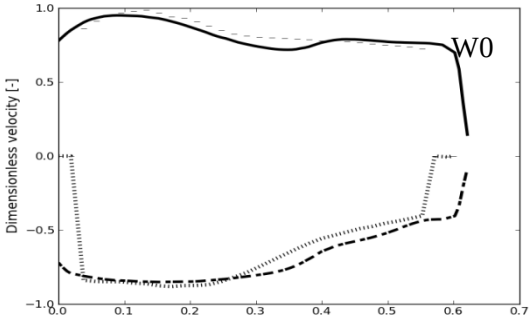

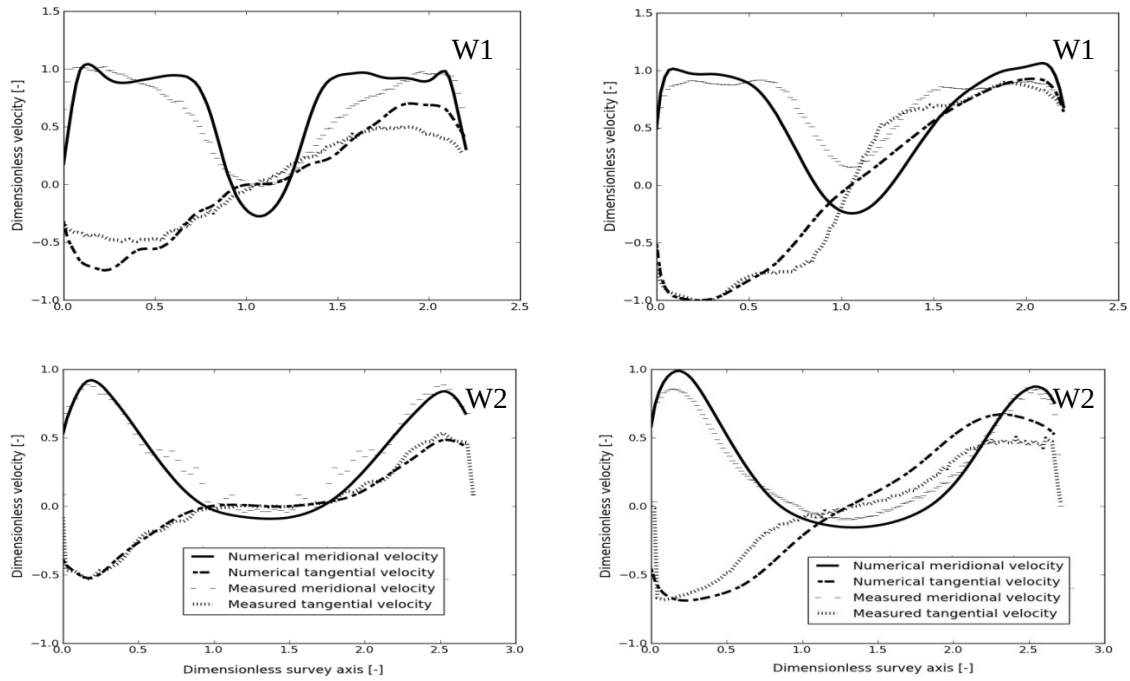

e) 800 *rpm* f) 925 *rpm*

Figure 4. Axial and tangential velocities, at W0, W1 and W2.

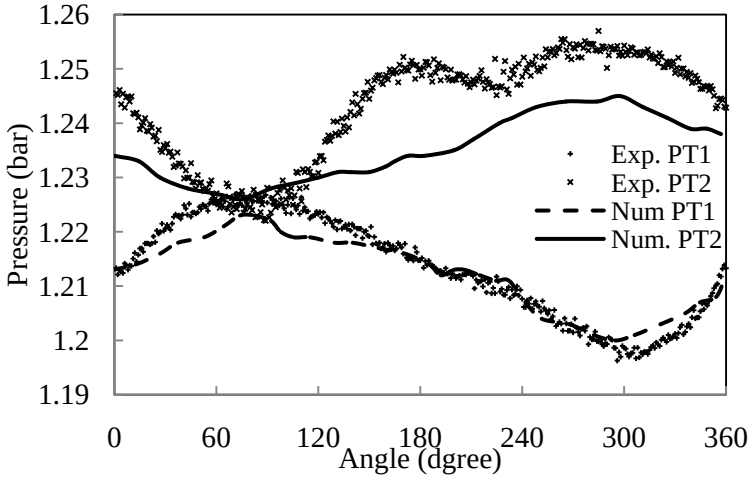

Figure 5. Phase-averaged pressure of the vortex rope for 925 *rpm* at two points in the cone.

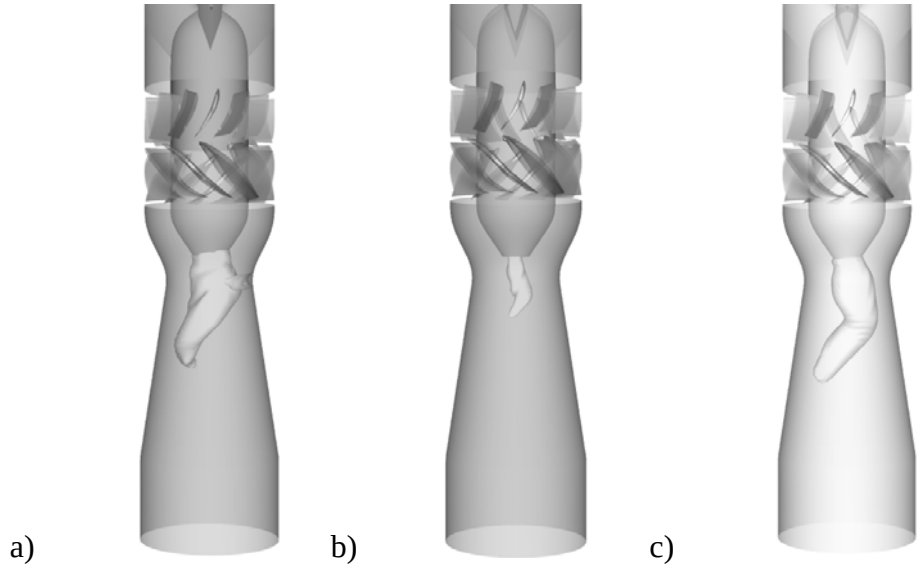

a) b) c)

Figure 6. Iso-surfaces of pressure for a) 400*rpm* b) 600*rpm* c) 925*rpm*.

4. Numerical results and validation

The numerical velocity is normalised by the bulk velocity at the throat and the axis of survey windows are normalised by the throat diameter. The numerical mean results are averaged over five complete runner revolutions. The flow Reynolds number based on the throat diameter and bulk velocity is 3.81×10^5.

The generated swirl in Fig. 4 is at its maximum level downstream of the runner blade and decays along the conical diffuser. The axial velocity at W0 is similar for all rotational speeds due to the constant mass flux and its independence of the rotational speed. The tangential velocity decreases linearly from hub to shroud, and is reverse of the runner rotation for the 400 *rpm* and 500 *rpm* cases. This is related to the reaction of the blade to the swirling flow from upstream. The rotational speed is not high enough to neutralize the incoming swirl, and the flow hits the blade and reflects in the opposite direction. This swirl, in opposite direction of the runner rotation, is the highest for the lowest rotational speed. The largest tangential velocity at W0 occurs for 400 *rpm* and close to the hub. As previously mentioned, the runner blade has a special shape, which close to the hub is pump-like and close to the shroud is turbine-like. Consequently, the inner part of the blade produces more swirl in lower rotational speeds, 400 *rpm* and 500 *rpm*, see Fig. 4. For 600 *rpm* and 700 *rpm*, the inner one third of the survey axis is in opposite direction and the outer part is in the same direction as runner. The special shape of the runner blade plays less important role in higher rotational speeds since the centrifugal force is the governing parameter. The mean velocity components for 600 *rpm* and 700 *rpm* are very similar in the cone. The tangential velocity is in same direction as runner for 800 *rpm* and upwards.

The axial velocity for 400 *rpm* and 500 *rpm* at W1 is very similar. There is a central stagnant region which still rotates in opposite direction of the runner. Since the tangential velocity is a bit stronger for 400 *rpm*, the on-axis recirculation region is slightly larger compared to 500 *rpm*. Cross-section W1 is close to the throat and smaller than W2, therefore the maximum velocity is larger, see Fig. 4. The on-axis recirculation region occupies most of cross section W2, which means increasing the surface area of the conical diffuser in off-design conditions does not increase the efficiency. The on-axis recirculation region is smaller and backflow is less strong for 600 *rpm* and 700 *rpm* due to less strong swirl. As can be seen at W1 for 600 *rpm* and 700 *rpm*, the rotational direction agrees with the runner rotation direction at the outer part and in reverse at the inner part, which emphasises two different rotational regions. When the rotational speed increases enough, for 800 *rpm* and upwards, the

absolute tangential velocity is stronger close to the shroud which can be related to the centrifugal force. This increase is linear and is proportional to the radius, $\partial P/\partial r=\rho V_\theta^2/r$.

Figure 5 shows the phase averaged pressure of the vortex rope at two points on the cone wall, PT1 at the throat and PT2 100 mm downstream of the first one, see Fig. 2. The pressure is sinus-like with an amplitude of 0.9kPa. The numerical results predict the pressure field qualitatively reasonable while the frequency of vortex rope and the amplitude of the pressure are slightly lower than the experimental ones.

Figure 6 shows iso-surfaces of the pressure for three different rotational speeds. The vortex rope for 400 *rpm* is the strongest one since the highest swirl occurs at that condition rotating in the opposite direction of the runner. There is very small vortex rope for 600 *rpm* and 800 *rpm* but for higher speeds it again forms and strengthens. It is worth mentioning that the swirl close to the hub at W0 directly influences the vortex rope. The tangential velocity at W0 close to the hub is almost zero in the cases for which the vortex rope disappears. There is no swirl at W2 for these cases, 700 *rpm* and 800 *rpm*, i.e. the swirl decays quickly and the on-axis recirculation region is smaller. Furthermore, the tangential velocity is almost zero close to the shroud in 500 *rpm* in W0, still there is a strong vortex rope and large on-axis recirculation region.

Table 2 shows the swirl number, as defined in eq. (1), at W0, W1 and W2, for different rotational speeds. The swirl number is decaying for 600 *rpm* and upwards. The swirl number for 400 *rpm* and 500 *rpm* increases along the cone and in the reverse direction of the runner. The minimum swirl occurs at W1 for 600 *rpm*.

Table 2.Numerical swirl number at different windows for different rotational speeds

	400*rpm*	500*rpm*	600*rpm*	700*rpm*	800*rpm*	925*rpm*
W0	0.39	0.21	0.31	0.91	1.66	2.48
W1	0.61	0.7	0.05	0.66	0.81	0.93
W2	0.66	0.38	0.19	0.28	0.46	0.53

5. Conclusions

The swirling flow configurations generated by a swirling flow apparatus are investigated experimentally and numerically. The unsteadiness in the draft tube with six different runner rotational speeds are measured using LDV and validated with RNG k-ε results. For conditions where the vortex rope disappears, the tangential velocity decreases and the numerical results show better agreement with the experimental results. In reverse, when the tangential velocity increases, the vortex rope is larger and an on-axis recirculation region is formed. In such cases the numerical results overpredict the recirculation region. The precessing vortex rope is rotating in opposite direction of the runner for 400 *rpm* and 500 *rpm*. The vortex rope disappears or is very small for 600 *rpm* and 700 *rpm*. The precessing vortex rope is rotating in the same direction as the runner for 800 *rpm* and 925 *rpm*. The numerical results capture a slightly lower frequency of the vortex rope than the experimental one, for 925 *rpm*.

Acknowledgements

The research presented was carried out as a part of the ‘‘Swedish Hydropower Centre – SVC’’. SVC is established by the Swedish Energy Agency, Elforsk and SvenskaKraftnät together with Luleå University of Technology, The Royal Institute of Technology, Chalmers University of Technology and Uppsala University, www.svc.nu.

The computational facilities are provided by C^{3}SE, the center for scientific and technical computing at Chalmers University of Technology, and SNIC, the Swedish National Infrastructure for Computing.

The Romanian team was supported by a grant of the Romanian National Authority for Scientific Research, CNCS – UEFISCDI, project number PNII-ID-PCE-2012-4-0634.

References

[1] Gyllenram W and Nilsson H 2008Design and validation of a scale-adaptive filtering technique for LRN turbulence modeling of unsteady flow, *ASMEJ Fluid Eng*, **130**(5)051401

[2] Susan-ResigaR, MunteanS and BosiocA 2008 Blade Design for Swirling Flow Generator, *in Proc. 4th German-Romanian workshop on turbomachinery hydrodynamics (GROWTH-4)*, (Stuttgart, Germany) 1-16

[3] Dörfler P, Sick M and Coutu A 2013 Flow-induced pulsation and vibration in hydroelectric machinery, *Springer-Verlag London*

[4] Bosioc A I, Resiga R,Muntean S and Tănasă C 2012 Unsteady pressure analysis of a swirling flow with vortex rope and axial water injection in a discharge cone,*ASMEJ Fluid Eng*,**134**(8), 081104, 1-11

[5] Tănasă C, Resiga R S, Muntean S and Bosioc A 2013 Flow-Feedback Method for Mitigating the Vortex Rope in Decelerated Swirling Flows, *ASMEJ. Fluids Eng.***135**(6), 061304, 1-11

[6] Frunzăverde D, Muntean S, Marginean G, Campian V, Marsavina L, Terzi R and Serban V 2010 Failure analysis of a Francis turbine runner, *IOP Conf. Ser.: Earth Environ. Sci.*, **12**, 012115, 1-15

[7] Gyllenram W, Nilsson H and Davidson L 2007 On the failure of the quasicylindrical approximation and the connection to the vortex breakdown in turbulent swirling flow, *Physics of Fluids*, **19**(4), 045108, DOI: 10.1063/1.2717724

[8] Javadi A and Nilsson H 2014, Comparative study of scale-adaptive and large-eddy simulation of highly swirling turbulent flow through an abrupt expansion, *27th IAHR Symposium on Hydraulic Machinery and Systems,* (submitted)

[9] Clausen P D, Koh S G and Wood D H 1993 Measurements of a Swirling Turbulent Boundary Layer Developing in a Conical Diffuser,*Exp Therm Fluid Sci*, **6**, 39–48

[10] Guo B, Langrish TAG and Fletcher DF 2002 CFD simulation of precession in sudden pipe expansion flows with low inlet swirl,*Appl Math Model.***26**(1), 1–15

[11] Zohir A E, Abdel Aziz A A and Habib M A 2011 Heat transfer characteristics in a sudden expansion pipe equipped with swirl generators,*Int J Heat Fluid Flow***32**, 352–361

[12] Ciocan G, Iliescu M, Vu T C, Nennemann B and Avellan F 2007 Experimental study and numerical simulation of the FLINDT draft tube rotating vortex *ASMEJ Fluid Eng*, **129**, 146-158

[13] Muntean S, Nilsson H and Susan-Resiga R 2009 3D numerical analysis of the unsteady turbulent swirling flow in a conical diffuser using Fluent and OpenFOAM, *in Proc. of the 3rd IAHR International Meeting of the Workshop on Cavitation and Dynamic Problems in Hydraulic Machinery and Systems*, (Brno, Czech Republic), 155 – 164

[14] Javadi A and Nilsson H 2014Unsteady numerical simulation of the flow in the U9 Kaplan turbine model, *27th IAHR Symposium on Hydraulic Machinery and Systems*, (submitted)

[15] Javadi A and Nilsson H 2014LES and DES of swirling flow with rotor-stator interaction, *in Proc. of the 5th Symposium of Hybrid RANS-LES method* (Texas A&M Univerisity, USA)

[16] Muntean S, Bosioc I A, Stanciu R, Tanasa C and Susan-Resiga R 2011 3D Numerical Analysis of a Swirling Flow Generator,*in Proc. of the 4th International Meeting on Cavitation and Dynamic Problems in Hydraulic Machinery and Systems*,(Belgrade, Serbia), 115-125

[17] Bosioc A I, Tănasă C, Muntean S, Susan-Resiga R and Vekas L 2014 Unsteady pressure measurements of decelerated swirling flow in a draft tube cone at lower runner speeds, *in Proc. of the 27th IAHR Symposium, Hydraulic Machinery and Systems* (submitted)

[18] Beaudoin M and Jasak H 2008 Development of a generalized grid interface for turbomachinery simulation with OpenFOAM, *Open source CFD International Conference*,(Berlin, Germany)